The Canadian Mineralogist
Vol. 36, pp. 1587-1594 (1998)

EFFECT OF TEMPERATURE ON THE STRUCTURES OF LIZARDITE-1*T* AND LIZARDITE-$2H_1$

STEPHEN GUGGENHEIM[1] AND WUDI ZHAN

Department of Earth and Environmental Sciences,
University of Illinois at Chicago, 845 West Taylor Street, Chicago, Illinois 60607, U.S.A.

ABSTRACT

Lizardite-1*T* from Val Sissone, Italy, and lizardite-$2H_1$ from the Monte dei Tre Abati ophiolite complex, Coli, Italy, were studied by single-crystal X-ray-diffraction methods to 480° and 525°C, respectively. The 1*T* polytype refined to a residual value *R* of 0.050 ($wR = 0.058$) at 480°C in space group $P31m$, and the $2H_1$ polytype refined to an *R* of 0.031 ($wR = 0.035$) at 525°C in space group $P6_3cm$. Mean thermal-expansion coefficients for the cell parameters are $a = b = 0.37 \times 10^{-5}$/deg, $c = 1.13 \times 10^{-5}$/deg for 1*T*, and $a = b = 0.70 \times 10^{-5}$/deg, $c = 1.67 \times 10^{-5}$/deg for $2H_1$. For the 1*T* polytype, ditrigonal ring distortions (tetrahedral rotation angle, α) change from –1.5 to near 0° from 20 to 480°C, whereas the α value for the $2H_1$ polytype decreases from 1.8 to 1.3° at near 300°C, and remains constant at 1.3° to 475°C. The O–O distances for O–H...O linkages across the interlayer increase linearly from 3.08(1) to 3.15(1) Å from 20 to 475°C for the $2H_1$ polytype. In contrast, the 1*T* polytype shows near-constant values for similar O–O distances of 3.06(1) Å to 360°C. From 360 to 480°C, this distance increases at nearly the same rate as with the $2H_1$ polytype, from 3.06 to 3.09(1) Å. On the basis of longer O–O distances, the $2H_1$ polytype exhibits weaker hydrogen bond linkages across the interlayer at all temperatures than the 1*T* polytype. Thermal expansion is related to optimum hydrogen bonding (O–H...O linkages) across the interlayer, which is affected by both thermal effects (dynamic displacements) and structural constraints. Structural constraints are predominantly controlled by tetrahedral rotation within the plane of the sheet and the consequent movement of basal atoms of oxygen, which results from an adjustment of the tetrahedral and octahedral sheets to different modes of thermal expansion. Thermal effects dominate over structural constraints for the $2H_1$ polytype. In contrast, it is tentatively concluded that structural adjustments dominate to about 300°C in the 1*T* polytype, above which thermal effects dominate because the tetrahedral sheet is extended fully and interlayer bonding has weakened sufficiently.

Keywords: lizardite, serpentine, high-temperature, structure, polytypes, hydrogen bonding, X-ray diffraction.

SOMMAIRE

Nous avons étudié la lizardite-1*T* provenant du Val Sissone, en Italie, et la lizardite-$2H_1$ provenant du massif ophiolitique de Monte dei Tre Abati, à Coli, en Italie, par diffraction X sur cristal unique jusqu'à 480° et 525°C, respectivement. La structure du polytype 1*T* a été affinée jusqu'à un résidu *R* de 0.050 ($wR = 0.058$) à 480°C dans le groupe spatial $P31m$, et celle du polytype $2H_1$, jusqu'à un résidu *R* de 0.031 ($wR = 0.035$) à 525°C dans le groupe spatial $P6_3cm$. Les coefficients d'expansion thermique des paramètres réticulaires *a* et *b* de la lizardite 1*T* sont 0.37×10^{-5}/deg, et de *c*, 1.13×10^{-5}/deg; ceux des paramètres *a* et *b* de la lizardite $2H_1$ sont 0.70×10^{-5}/deg, et de *c*, 1.67×10^{-5}/deg. La distorsion des anneaux ditrigonaux dans le polytype 1*T* (angle de rotation des tétraèdres, α) varie de –1.5 à presque 0° entre 20 et 480°C, tandis que la valeur de α pour le polytype $2H_1$ diminue de 1.8 à 1.3° près de 300°C, et demeure constant à 1.3° jusqu'à 475°C. Les distances O–O des agencements O–H...O perpendiculaires à la couche interfeuillet augmentent de façon linéaire de 3.08(1) à 3.15(1) Å en allant de 20 à 475°C dans le cas du polytype $2H_1$. En revanche, le polytype 1*T* fait preuve de distances O–O quasi constantes, 3.06(1) Å, jusqu'à 360°C. Entre 360 et 480°C, cette distance augmente à environ le même taux que dans le polytype $2H_1$, de 3.06 à 3.09(1) Å. A cause des plus grandes distances O–O, le polytype $2H_1$ aurait des liaisons hydrogène plus faibles perpendiculaires aux feuillets que la lizardite-1*T*, et ce, sur l'intervalle complet de températures. L'expansion thermique est liée au réseau de liaisons hydrogène (O–H...O) perpendiculaires à la couche inter-feuillet, qui est régi à la fois par des effets thermiques (déplacements dynamiques) et des contraintes structurales. Ces dernières reflètent surtout la rotation des tétraèdres dans le plan du feuillet et le mouvement conséquent des atomes d'oxygène à la base du feuillet, qui résulte d'un ajustement des feuillets de tétraèdres et d'octaèdres aux modes variés d'expansion thermique. Les effets thermiques sont plus importants que les contraintes structurales dans le polytype $2H_1$. Les ajustements structuraux seraient prédominants jusqu'à environ 300°C dans le polytype 1*T*, et au-delà de ce seuil, ce sont les effets thermiques qui prédominent parce que le feuillet de tétraèdres est complètement distendu, et les liaisons interfeuillets affaiblies davantage.

Mots-clés: lizardite, serpentine, température élevée, structure, polytypes, liaisons hydrogène, diffraction X.

[1] *E-mail address*: xtal@uic.edu

Introduction

The Mg-rich serpentine minerals are important geologically because they occur over a broad range of temperatures and pressures, from lower zeolite to upper greenschist facies. In addition, however, serpentines occur in subduction zones and are often regarded as a potential repository for H_2O or hydrogen in the upper mantle (*e.g.*, Prewitt & Finger 1992). Furthermore, Mg-rich serpentines are significant from a crystal-chemical view; they form a complex group of minerals ranging in morphology and structure from cylinders, to coils, to corrugated waves, and to plates. Intergrowths between the various serpentine-group minerals occur frequently, and disequilibrium conditions, as indicated by textural and chemical inhomogeneities, are common. Thus, understanding the structural interrelationships among the serpentines is critical to understand the possible role of kinetics, composition, bonding characteristics, and environmental factors such as temperature and pressure, in forming these phases.

Until the early 1980s, suitable crystals for high-quality structural work were unavailable for any of these serpentines. Since then, however, Mellini and coworkers (Mellini 1982, Mellini & Zanazzi 1987, 1989, Mellini & Viti 1994) studied structurally two polytypes of the platy Mg-rich serpentine *lizardite* (lizardite-1*T* and -$2H_1$). In addition, Brigatti *et al.* (1997) examined the $2H_2$ form of lizardite. Mellini & Zanazzi (1989) determined structurally the effect of pressure on lizardite-1*T*, and Gregorkiewitz *et al.* (1996) reported a neutron-diffraction study using Rietveld refinement at low temperatures on similar material. To complete the series and to describe fully the lizardite structure, we report the high-temperature structures of lizardite-1*T* and -$2H_1$ by single-crystal X-ray methods.

High-Temperature Single-Crystal Studies of Phyllosilicates

There have been few high-temperature structural studies of phyllosilicates (Takeda & Morosin 1975, Guggenheim *et al.* 1987, Nelson & Guggenheim 1993). Of these studies, only the recent study on chlorites (Nelson & Guggenheim 1993) examined a phyllosilicate structure at high temperature in which hydrogen bonding plays an important role in bonding adjacent layers. In that study, Nelson & Guggenheim (1993) found that (1) the axial lengths in chlorites do not necessarily expand most rapidly along the *c* axis, (2) the interlayer regions in which H bonding is most prevalent do not expand very rapidly, although H bonds are generally considered weak bonds, and (3) electrostatic attractions between layers may be key in determining expansion behavior in phyllosilicates. Nelson & Guggenheim (1993) discussed also the mechanisms of oxidation in Fe-bearing chlorites.

Lizardite, similar to chlorite, has strong layer-to-layer interactions by both a network of H-bonds and strong electrostatic interactions. These electrostatic interactions originate from a net negative charge from the ideal on the tetrahedral sheet and a net positive charge from the ideal on the octahedral sheet. We examine two polytypes of lizardite with similar chemical compositions, but different networks of H-bonds, to determine the effect of temperature on the structure of this important serpentine-group mineral.

Experiments and Results

Lizardite-1*T* from Val Sissone, Italy (Mellini 1982) and lizardite-$2H_1$ from the Monte dei Tre Abati ophiolite complex, Coli, Italy (Boscardin *et al.* 1982, Mellini & Zanazzi 1987) were studied. Chemical data (Mellini 1982) for the *1T* sample are: $(Mg_{2.79}Fe^{2+}_{0.04}\ Fe^{3+}_{0.10}\ Al_{0.07})_{\Sigma 3.00}(Si_{1.83}Al_{0.17})_{\Sigma 2.00}O_5(OH)_4$ and for the $2H_1$ crystal (Mellini & Zanazzi 1987) are: $(Mg_{2.83}Fe^{2+}_{0.05}\ Al_{0.10})_{\Sigma 2.98}(Si_{1.93}Al_{0.07})_{\Sigma 2.00}O_5(OH)_4$. Buerger precession photographs indicate that there is no significant stacking disorder in any of the crystals examined, although the $2H_1$ polytype material was of better quality than the 1*T* crystals. Crystals of each were selected, with the 1*T* crystal approximately 0.1 × 0.1 × 0.07 mm in size and the $2H_1$ crystal 0.07 × 0.07 × 0.05 mm. In accord with the previous room-temperature structures (Mellini 1982, Mellini & Zanazzi 1987), Buerger precession camera data indicated that the space group is $P31m$ and $P6_3cm$ for the 1*T* and $2H_1$ crystals, respectively. The 1*T* crystal used in the refinement showed a small amount of mosaic spread, suggesting that incipient cleavage had developed, whereas the $2H_1$ sample showed only very sharp reflections.

Each crystal was mounted in a Na-poor, silica-rich capillary ("quartz glass"), sealed at one end, so that the crystal was fixed at the sealed end of the capillary for collection of the high-temperature data. A second capillary, telescoping within the first, was placed so that it touched the crystal, thereby firmly securing it in place. A dot of the liquid fraction of Zircoa Bond 6 was used to fix the inner capillary in place to the outer capillary, but care was taken not to seal all the space between the two capillaries so that the capillaries could be evacuated. The capillaries were allowed to dry for 10 hours, then simultaneously evacuated and heated at 100°C for 15 minutes to remove water vapor, and then sealed with an acetylene torch. The assembly was then mounted on a goniometer for single-crystal work.

An automated Picker four-circle, single-crystal X-ray diffractometer equipped with a single-crystal furnace (Brown *et al.* 1973), was used with graphite monochromatized Mo$K\alpha$ ($\lambda = 0.71069$ Å) radiation for data measurement. The furnace was calibrated following the method of Guggenheim *et al.* (1987) after the method of Brown *et al.* (1973), using the melting points

of phenolthalein (261°C), $NaNO_3$ (307°C), $Ba(NO_3)_2$ (592°C), $MgCl_2$ (708°C), and KCl (790°C). The temperature was monitored with a Tempstar III temperature controller. The estimated error in temperature is ±3°. Each temperature was allowed to equilibrate for a minimum of 3 h before data collection was initiated. Using *least-squares* refinement of 23 reflections taken at each octant (23 × 8 = 184 measured positions) for the 1*T* sample and 18 reflections (144 positions) for the $2H_1$ sample, cell parameters were determined at 20, 150, 270, 360, 440, 480°C for the 1*T* polytype and at 20, 150, 200, 250, 300, 350, 400, 475, 525°C for the $2H_1$ polytype (Table 1). Full datasets for structural analysis were collected at room temperature, 360, and 480°C for 1*T* and at room temperature, 300, and 475°C for the $2H_1$ crystals. For data collection, half of the limiting sphere was sampled over the ranges $-7 \le h \le 7$, $0 \le k \le 12$, and $-12 \le l \le 12$ for the 1*T* polytype, and $-7 \le h \le 7$, $0 \le k \le 12$, and $-24 \le l \le 24$ for the $2H_1$ polytype, with a scan rate of 1°C/min, scan window of 2.0° + 0.75tanθ, and a background time of one half the scan time per background measurement. The 2θ:θ fixed-scan mode was used, with three standard reflections monitored every 360 minutes (approximately every 60 reflections) for electronic stability. Reflections were considered observed if I exceeded 3σ, where $(I) = [CT + 0.25(t_c/t_b)^2(B_1 + B_2) + pI)^2]^{1/2}$, and where CT is the total integrated count in time t_c, B_1 and B_2 are the background counts in time t_b, and p (the estimate of the standard error) = 0.03. Lorentz-polarization corrections were made, and absorption effects were corrected empirically by using Ψ scans. Reflections selected for Ψ scans were chosen to be representative of the θ and χ values of the reflections in the dataset, and scans were made in Ψ at 10° increments. Approximately 350 reflections were used to produce correction coefficients (using SHELXTL PLUS 4.0, Siemens 1990) to correct the raw data. Psi scans were made at room temperature only and were applied to higher-temperature datasets also.

Atomic parameters (Mellini & Zanazzi 1987) of the 1*T* and $2H_1$ polytype were used initially for the room-temperature dataset. Scattering factors were calculated using the method of Sales (1987) and the tables of Cromer & Mann (1968), assuming half-ionization of atoms. The least-squares refinement program SHELXTL PLUS (Siemens 1990) was used, and reflections were assigned unit weights and a single scale-factor. For the first several cycles, only isotropic-displacement factors were applied, followed by anisotropic-displacement factors. The atomic parameters at room temperature were used initially for the high-temperature refinements, and the procedures for the high-temperature refinements were similar to those at room temperature. Final *R* factors and other results are given in Table 2. The H atoms were located by difference-Fourier syntheses for both cases, and the locations were not refined. Atomic coordinates and displacement parameters are given in Table 3, and bond distances are given in Table 4.

TABLE 1. UNIT-CELL PARAMETERS OF LIZARDITE-1*T* AND LIZARDITE-$2H_1$ AS A FUNCTION OF TEMPERATURE

T(°C)	*a*(Å)	*c*(Å)	V(Å³)	T(°C)	*a*(Å)	*c*(Å)	V(Å³)
	1T				$2H_1$		
20	5.326(3)	7.288(5)	179.1(2)	20	5.317(4)	14.551(3)	356.3(3)
150	5.327(3)	7.314(6)	179.8(2)	150	5.333(4)	14.578(2)	359.0(3)
270	5.330(3)	7.313(6)	180.0(2)	250	5.334(4)	14.600(2)	359.7(3)
360	5.333(4)	7.324(5)	180.4(2)	300	5.336(4)	14.614(2)	360.4(3)
440	5.331(4)	7.324(5)	180.3(1)	350	5.340(4)	14.626(2)	361.1(3)
480	5.332(3)	7.332(5)	180.5(2)	400	5.342(4)	14.651(2)	362.0(3)
				475	5.345(4)	14.662(2)	362.6(4)
				525	5.345(4)	14.674(2)	363.0(3)

Discussion

Mellini (1982) and Mellini & Zanazzi (1987) discussed stability of flat-layer (lizardite) polytypes on the basis of the misfit between component tetrahedral and octahedral sheets, the effect of isomorphous substitution and resulting electrostatic interactions between adjacent tetrahedral and octahedral sheets across the interlayer (Gillery 1959), and the formation of the hydrogen-bond network. Mellini (1982) and Mellini & Zanazzi (1987) suggested that the latter two mechanisms are the most important for stability.

Unit-cell parameters

Table 1 and Figure 1 show the effect of temperature on unit-cell parameters and volume for the two polytypes. For purposes of comparison, the *c* axis of the $2H_1$ polytype is given as *c*/2 in Figure 1a. The 150°C value for the *c* axis of the 1*T* form appears inconsistent with the other data. Thus, it is omitted in the determination of the linear regression fit of the data. Note that the axial lengths increase with increasing temperature, and the rate of expansion differs considerably for the two forms. The cell lengths of the $2H_1$ form increase as a function of temperature at a greater rate than the 1*T* form [see Table 5 for mean thermal-expansion coefficients

TABLE 2. RESULTS OF STRUCTURAL REFINEMENTS OF LIZARDITE-1*T* AND LIZARDITE-$2H_1$ AT VARIOUS TEMPERATURES

	1T			$2H_1$		
	20°C	360°C	480°C	20°C	300°C	475°C
R1*	0.052	0.058	0.050	0.033	0.045	0.31
*w*R**	0.064	0.070	0.058	0.037	0.054	0.035
Goodness-of-fit§	1.06	0.93	0.78	1.20	1.72	1.16
Variable parameters	36	30	36	36	29	36
Data set	186	175	167	169	169	164

* R1 = $(||Fo| - |Fc||)/|Fo|$.

** *w*R2 = $\{[w(|Fo| - |Fc|^2]/w|Fo|^2\}^{1/2}$, where $w = 1$.

§ Goodness-of-fit: $[w||Fo| - |Fc||^2/(n - m)]^{1/2}$, where *n* represents the number of independent data, and *m* is the number of parameters.

TABLE 3. POSITIONAL COORDINATES AND DISPLACEMENT PARAMETERS FOR LIZARDITE-1*T* AND LIZARDITE-2H_1

Atom	*x*	*y*	*z*	U_{11}	U_{22}	U_{33}	U_{23}	U_{13}	U_{12}
				Lizardite-*1T* at 20^0 C					
Mg	0.3318(9)	0.0	0.455(1)	3(2)	3(2)	22(2)	0.0	-2(1)	$U_{22}/2$
Si	0.3333	0.6667	0.074(1)	6.5(9)	6.5(9)	26(1)	0.0	0.0	
O1	0.3333	0.6667	0.2911*	3(2)	3(2)	36(2)	0.0	0.0	
O2	0.507(2)	0.0	-0.008(1)	14(2)	7(2)	21(2)	0.0	-2(2)	
O3	0.664(2)	0.0	0.588(1)	9(2)	8(2)	22(2)	0.0	-2(2)	
O4	0.0	0.0	0.304(2)	8(2)	8(2)	13(2)	0.0	0.0	
H1	0.583	0.0	0.732						
H2	0.0	0.0	0.197						
				Lizardite-*1T* at 360^0 C					
Mg	0.3327(9)	0.0	0.456(1)	8(1)	7(2)	29(2)	0.0	-1(2)	$U_{22}/2$
Si	0.3333	0.6667	0.077(1)	8.9(9)	8.9(9)	34(2)	0.0	0.0	
O1	0.3333	0.6667	0.2918*	10(2)	10(2)	29(3)	0.0	0.0	
O2	0.501(2)	0.0	-0.007(2)	19(2)	9(2)	33(3)	0.0	-1(3)	
O3	0.662(2)	0.0	0.592(2)	18(2)	15(3)	24(2)	0.0	-0(3)	
O4	0.0	0.0	0.303(2)	20(3)	20(3)	26(3)	0.0	0.0	
				Lizardite-*1T* at 480^0 C					
Mg	0.3321(8)	0.0	0.457(1)	11(1)	11(1)	34(2)	0.0	0.1(1)	$U_{22}/2$
Si	0.3333	0.6667	0.078(1)	12.6(8)	12.6(8)	36(2)	0.0	0.0	
O1	0.3333	0.6667	0.2914*	15(2)	15(2)	30(2)	0.0	0.0	
O2	0.500(2)	0.0	-0.005(1)	23(2)	13(2)	37(2)	0.0	-3(2)	
O3	0.664(2)	0.0	0.592(1)	22(2)	20(2)	25(2)	0.0	1(2)	
O4	0.0	0.0	0.306(2)	22(2)	22(2)	28(3)	0.0	0.0	
H1	0.572	0.0	0.730						
H2	0.0	0.0	0.190						
				Lizardite-2H_1 at 20^0 C					
Mg	0.3327(8)	0.0	0.2225(5)	11(2)	9(2)	19(1)	0.0	-1(1)	$U_{22}/2$
Si	0.3333	0.6667	0.0314(5)	8.7(9)	8.7(9)	11(1)	0.0	0.0	
O1	0.3333	0.6667	0.1406*	10(2)	10(2)	24(2)	0.0	0.0	
O2	0.491(2)	0.0	-0.0070(6)	20(2)	20(2)	28(2)	0.0	-13(3)	
O3	0.666(1)	0.0	0.2896(6)	19(2)	24(2)	8(2)	0.0	-3(3)	
O4	0.0	0.0	0.1470(9)	16(2)	16(2)	13(3)	0.0	0.0	
H1	0.622	0.0	0.354						
H2	0.0	0.0	0.075						
				Lizardite-2H_1 at 300^0 C					
Mg	0.332(2)	0.0	0.2188(8)	18(2)	15(4)	18(2)	0.0	-0(3)	$U_{22}/2$
Si	0.3333	0.6667	0.0292(7)	13(2)	13(2)	12(2)	0.0	0.0	
O1	0.3333	0.6667	0.1406*	23(5)	23(5)	15(5)	0.0	0.0	
O2	0.494(5)	0.0	-0.009(1)	38(6)	29(6)	30(5)	0.0	-14(18)	
O3	0.667(3)	0.0	0.2859(9)	24(5)	25(9)	31(6)	0.0	-2(9)	
O4	0.0	0.0	0.144(2)	20(7)	20(7)	26(11)	0.0	0.0	
				Lizardite-2H_1 at 475^0 C					
Mg	0.3319(9)	0.0	0.2243(5)	18(1)	17(2)	28(1)	0.0	-1(2)	$U_{22}/2$
Si	0.3333	0.6667	0.0344(5)	15(1)	15(1)	17(1)	0.0	0.0	
O1	0.3333	0.6667	0.1437*	21(2)	21(2)	20(2)	0.0	0.0	
O2	0.493(2)	0.0	-0.0023(6)	36(2)	27(2)	31(2)	0.0	-12(3)	
O3	0.668(2)	0.0	0.2909(6)	31(2)	31(2)	21(2)	0.0	3(2)	
O4	0.0	0.0	0.149(1)	25(2)	25(2)	25(2)	0.0	0.0	
H1	0.621	0.0	0.343						
H3	0.0	0.0	0.068						

Anisotropic displacement factors (x 10^3) are in the form $\exp[-2\pi^2(\Sigma_i \Sigma_j h_i h_j a^*_i a^*_j U_i U_j)]$. *Esds* in parentheses.
*Defines origin along *c* axis and thus, not refined.

TABLE 4. SELECTED BOND-LENGTHS AND ANGLES, LIZARDITE-1*T* AND LIZARDITE-2H_1

	Bond lengths (Å)			Bond angles(°)	
		Lizardite-*1T*			
	20°C	480°C		20°C	480°C
Si-O1	1.581(8)	1.563(7)	O2-Si-O1 x3	111.3(4)	111.6(4)
Si-O2 x3	1.651(5)	1.655(5)	O2-Si-O2 x3	107.6(5)	107.3(4)
Mean	1.634	1.632		109.5	109.5
O1-O2 x3	2.669(9)	2.662(9)			
O2-O2 x3	2.664(2)	2.666(2)			
Mean	2.667	2.664			
Mg-O3	2.019(10)	2.026(10)	O3-Mg-O1 x2	84.4(2)	84.9(2)
Mg-O4	2.081(9)	2.087(9)	O4-Mg-O1 x2	93.5(3)	93.1(2)
Mg-O1 x2	2.142(5)	2.156(5)	O1-Mg-O1 x2	84.2(2)	84.7(2)
Mg-O3 x2	2.029(7)	2.036(7)	O1-Mg-O3 x2	98.3(4)	98.0(4)
Mean	2.074	2.083	O3-Mg-O4 x2	83.6(3)	83.8(3)
			O1-Mg-O1	91.7(3)	91.1(3)
Across interlayer			O3-Mg-O3	99.7(6)	99.3(6)
O2-O3	3.06(1)	3.09(1)			
		Lizardite-2H_1			
	20°C	475°C		20°C	475°C
Si-O1	1.588(7)	1.603(7)	O2-Si-O1 x3	109.9(4)	109.2(4)
Si-O2 x3	1.636(4)	1.634(4)	O2-Si-O2 x3	109.0(4)	109.7(4)
Mean	1.624	1.626		109.5	109.5
O1-O2 x3	2.640(8)	2.639(7)			
O2-O2 x3	2.663(2)	2.673(2)			
Mean	2.652	2.656			
Mg-O3	2.027(9)	2.042(10)	O3-Mg-O1 x2	84.5(2)	84.0(2)
Mg-O4	2.085(9)	2.091(10)	O4-Mg-O1 x2	93.4(3)	93.7(3)
Mg-O1 x2	2.139(5)	2.141(5)	O1-Mg-O	91.9(3)	92.2(3)
Mg-O3 x2	2.025(7)	2.026(7)	O3-Mg-O3 x2	98.6(4)	98.9(4)
Mean	2.073	2.078	O3-Mg-O4 x2	83.3(3)	83.3(3)
			O1-Mg-O1 x2	84.5(2)	84.4(2)
Across interlayer			O3-Mg-O3	98.9(5)	98.8(5)
O2-O3	3.08(1)	3.15(1)			

TABLE 5. MEAN COEFFICIENTS OF THERMAL EXPANSION FOR POLYHEDRA AND SHEET THICKNESS*

	1T	2H_1		*1T*	2H_1
	$\alpha_{20\text{-}480}$	$\alpha_{20\text{-}475}$		$\alpha_{20\text{-}480}$	$\alpha_{20\text{-}475}$
	Silicon tetrahedra			Octahedral sites	
Si-O1	-0.25	2.01	Mg-O3'	0.75	1.60
Si-O2	0.05	-0.27	Mg-O4	0.63	0.63
Mean Volume	-0.27	0.27	Mg-O1	1.42	0.20
			Mg-O3'	0.75	0.11
			Mean Volume	0.94	0.53
	Interlayer separation				
	0.59	5.37			
	Cell parameters				
$a = b$	0.37	0.70			
c	1.13	1.67			
Volume	1.70	2.99			

* $\times 10^{-5}$/degree. Note that the mean coefficients of thermal expansion, α, are calculated from $\alpha = (1/X_{20})[(XT - X_{20})/(T - 20)]$, where X_{20} and XT are the values of the parameter at room temperature (20°C) and at higher temperature, XT, respectively. Wherever possible, α is calculated using the slope of the linear regression analysis for the term $[(XT - X_{20})/(T - 20)]$. Differences in the values between the 1*T* and 2H_1 forms for Si and Mg bonds are probably not significant.

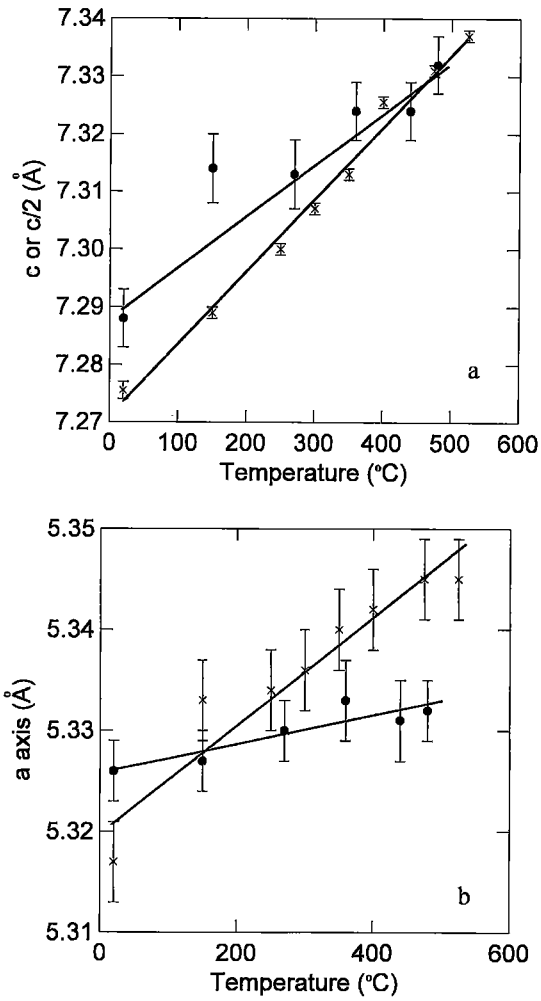

FIG. 1. (a) Plot of *c* or *c*/2 *versus* temperature for lizardite-1*T* (circles) and lizardite-2H_1 (crosses). (b) Plot of *a versus* temperature (symbols as before).

(MTEC) values of *a* and *c* for 1*T*: 0.27×10^{-5}, 1.11×10^{-5}; 2H_1: 0.98×10^{-5}, 1.73×10^{-5}]. The MTEC values for the 1*T* form are consistent with values derived from the low-temperature data of Gregorkiewitz *et al.* (1996).

The reported room-temperature cell parameters (Mellini & Zanazzi 1987) for the 2H_1 sample [*a* 5.318(4), *c* 14.541(7) Å] are in close agreement with those reported here [*a* 5.317(4), *c* 14.551(3) Å]. However, the *c* parameter for the 1*T* polytype in this study [*a* 5.326(3), *c* 7.288(5) Å] differs significantly from that reported by Mellini (1982) [*a* 5.332(5), *c* 7.233(7) Å]. In a Rietveld study of a lizardite-1*T* sample from Elba, Gregorkiewitz *et al.* (1996) reported the room-temperature cell parameters *a* and *c* to be 5.3332(2) and 7.2718(6) Å respectively, which is more consistent with the data of this study. Thus, the differences in the *c* cell

dimension of the 1*T* sample between this study and that of Mellini (1982) may be related to problems in the Mellini determination, to difficulties due to the mosaic spread (see above) in this study, or to slight differences in composition between the two samples. Unfortunately, the 1*T* crystal was lost after data collection, and the precise composition of the crystal could not be determined.

Substitution of R^{3+} for R^{2+} in the octahedral sheet produces a net positive charge, and substitutions of R^{3+} for R^{4+} in the tetrahedral sheet produce a net negative charge in lizardite, although the layer as a whole is neutral. Because layer surfaces oppose each other across the interlayer space and these surfaces have opposite net charges, Gillery (1959) argued that the basal spacings [*e.g.*, *d*(001)] will decrease with increasing R^{3+} substitution. In fact, interlayer separation (Table 6) is the more critical distance than basal spacing to judge the effects of electrostatic interactions between the layer surfaces. It is noteworthy that the interlayer separations for the 1*T* sample are smaller than the $2H_1$ sample at comparable temperatures. Thus the data support the suggestion by Gillery (1959), although there may be uncertainty about the *c* parameter (or composition) of the 1*T* sample reported here.

Network of hydrogen-bonds

Obtaining accurate atomic locations for H atoms, even at room temperature, using X-ray data is difficult.

TABLE 6. ADDITIONAL STRUCTURAL DETAILS FOR LIZARDITE-1*T* AND LIZARDITE-$2H_1$ AT VARIOUS TEMPERATURES

	1*T*			$2H_1$		
parameter	20°C	360°C	480°C	20°C	300°C	475°C
α(°)*	–1.5	–0.2	0.05	1.8	1.3	1.3
τ(°)**	111.3	111.7	111.6	110.0	109.7	109.2
ψ(°)§	59.06	58.62	8.60	58.92	59.39	59.12
Sheet thickness (Å)						
Tetrahedra	2.180	2.190	2.170	2.178	2.198	2.166
Octahedra	2.133	2.170	2.170	2.138	2.106	2.133
Interlayer separation (Å)	2.944	2.936	2.955	2.959	3.004	3.032
Polyhedral site volumes (Å^3)						
Octahedra	11.66	11.87	11.83	11.63	11.53	11.73
Tetrahedra	2.24	2.25	2.23	2.19	2.24	2.21
Polyhedral site quadratic elongation (λ)¶						
Octahedra	1.014	1.012	1.012	1.013	1.015	1.014
Tetrahedra	1.001	1.002	1.002	1.000	1.000	1.000

* tetrahedral rotation angle, $\alpha = |120° - (\text{mean } O_b\text{–}O_b\text{–}O_b \text{ angle})|$

** tetrahedral elongation, $\tau = O_{apical}\text{–}T\text{–}O_{basal}$, where the ideal value is 109.47°.

§ octahedral distortion, $\psi = \cos^{-1}[\text{oct. thickness}/2(\text{mean Mg–O,OH})]$, where the ideal value is 54.73°.

¶ $\lambda = \Sigma[(l/l_0)^2/n]$, where l_0 is the *M*–O or *T*–O distance of a regular polyhedron of the same volume; l is the *M*–O or *T*–O distance, and n is the coordination number (Robinson *et al.* 1971). A regular polyhedron has a value of 1.0.

Phyllosilicates structures are especially problematic because reflection profiles are affected by errors in stacking periodicity and incipient cleavage. Also, there are severe adsorption effects due to the platy shape of the sample. Add the additional complications of furnace arrangement, mounting procedures for high temperature, and the effects of temperature on the H, and it is unlikely that determined H positions (and displacement factors) at high temperature are accurate. Note that the refinements at the intermediate temperatures for both samples have the greatest *R* values and the largest estimated standard deviations (*esd*); no coordinates of H atoms are given for these temperatures.

Mellini (1982) emphasized the importance of the H-bonding network in the formation of platy polytypes. He noted that polytype stability increases with strong interlayer bonding, which is favored by certain configurations of the layers, such as the 1*T* and $2H_1$ polytypes, and the direction (±) of tetrahedron rotation (*i.e.*, ditrigonal distortion). Mellini noted further, and we agree, that the magnitude of tetrahedron rotation (α) caused by misfit between the tetrahedral and octahedral sheets is less important than the H-bonding network in understanding the development of polytypes.

In contrast, however, the network of H-bonds at high temperatures will be significantly influenced by both the direction and magnitude of tetrahedron rotation. At higher temperatures for a given crystal, the magnitude of tetrahedron rotation must approach zero more closely to allow for lateral expansion of the octahedra (Table 6), since lateral expansion of a tetrahedron is minimal. Thus, optimum H bonding in lizardite at elevated temperatures involves the combination of effects caused by expansion along *c** and torsional effects from tetrahedron rotation, much like that found in chlorites (Nelson & Guggenheim 1993). Although accurate locations of the H positions are useful to better understand torsional effects, the O–O distances of the O–H...O are nonetheless sufficient to determine approximately how the H influences linkages between the layers.

For lizardite-1*T*, α closely approaches zero with increasing temperature (Fig. 2), thereby suggesting that the tetrahedral sheet has reached the limit of its extension by 350–500°C (errors associated with these angles are ±0.25°). Lizardite-$2H_1$ also shows an approach in α toward zero (to 1.3°) at high temperature, but the tetrahedral sheet does not require full extension for sheet congruency to the octahedral sheet. In addition, the α value for the $2H_1$ polytype is not affected by temperature above 300°C.

Figure 3 shows O–O distances associated with the H bond across the interlayer for both polytypes. Although tetrahedron rotations for the $2H_1$ polytype do not change significantly above 300°C, the O–O separation continues to enlarge. For the $2H_1$ polytype, this suggests that thermal effects (*e.g.*, atom displacements) dominate above 300°C over structural constraints to maintain an optimum network of H-bonds. Because the slope of the

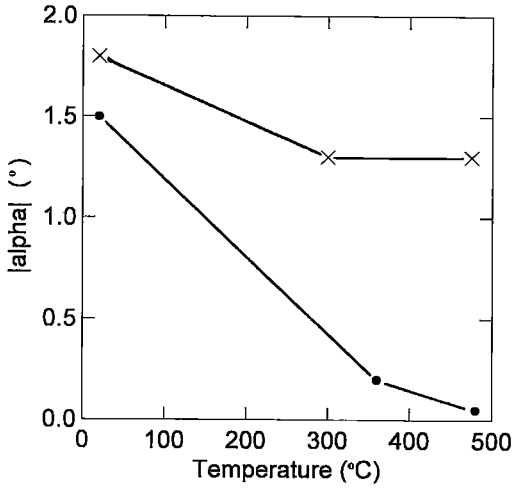

FIG. 2. The absolute value of the tetrahedral rotation angle, | α |, *versus* temperature (circles: 1*T*, crosses: $2H_1$).

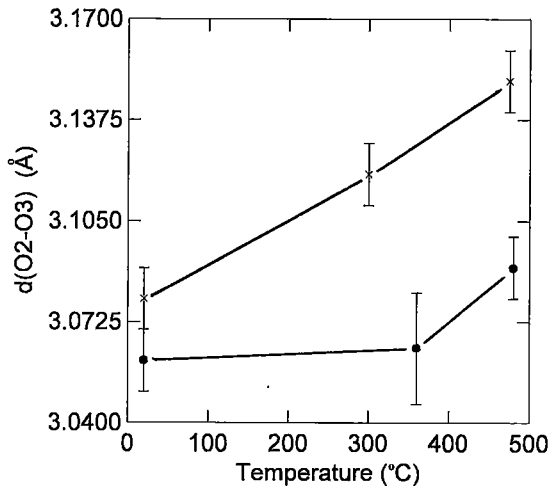

FIG. 3. O–O distances across the interlayer associated with the H atom (circles: 1*T*, crosses: $2H_1$).

curve remains the same over the entire range of temperatures studied, thermal effects are dominant at all temperatures.

In contrast, the 1*T* polytype behaves differently, although the following conclusions are tentative because the standard deviation of the O(2)–O(3) distance across the interlayer at 360°C is high [3.064(18) Å]. The rapid decline in the α value and the nearly constant O(2)–O(3) distance to about 300°C suggest that an optimum H-bonding network connecting the layers is maintained by structural adjustments primarily involving tetrahedron rotation. Above about 300°C, the O–O distances across the interlayer enlarge, suggesting that thermal effects become dominant because tetrahedron rotation can no longer act to maintain the system of H-bonds. It is noteworthy that the slope of the curve (Fig. 3) above 350°C for the 1*T* polytype nearly parallels that of the $2H_1$ polytype.

Rigid-body analysis

A rigid-body thermal analysis (Downs *et al.* 1992) may be important to understand the effect of potential misfit between the octahedral and tetrahedral sheets at high temperature, since bond distances in tetrahedra and octahedra may be affected by TLS (translational, librational, and screw) modes of motion. Rigid-body behavior requires that the difference in the mean square displacement amplitudes ($\mu_2 - \mu_1$) of two atoms along the bond must be relatively small, less than 0.002 Å^2 (Downs *et al.* 1990). For lizardite-$2H_1$, the three Si–O(2) bonds associated with the tetrahedra have values of ($\mu_2 - \mu_1$) of 0.012, almost an order of magnitude larger than expected for rigid-body behavior. Thus, the data show that a thermal motion correction based upon the rigid-body model cannot be applied. Reasons for this behavior may be related to several factors: (1) the tetrahedra are indeed "soft", with non-fixed interatomic separations oscillating about a mean; (2) small systematic errors in the data, possibly relating to incompletely applied absorption corrections (due to the platy shape and limitations caused by the furnace assembly), and (3) a static disorder (*e.g.*, substitutional and positional disorder, stacking errors, *etc.*) perhaps related to interactions between octahedra and tetrahedra caused by the semi-independent sheets.

Because Downs *et al.* (1992) demonstrated that SiO_4 tetrahedra for both chain and framework silicates are rigid at temperatures to 1100°C, it is unlikely that the tetrahedra are "soft"; there is no reason to expect that phyllosilicates differ. Incompletely applied absorption corrections for flat plates are problematic and cannot be ruled out. However, because variations in bond lengths caused by substitutions in the tetrahedra and octahedra will affect positions of basal oxygen atoms and such variations are common for all but end-member compositions, then a thermal motion correction will not be applicable to those phyllosilicates with static disorder derived from isomorphous substitutions. To determine whether absorption effects or static disorder account for the large mean-square displacement amplitudes, future high-temperature studies should consider multiple absorption-correction strategies to minimize possible errors due to absorption.

Conclusions

This study shows that variations in stacking sequence affect the structural response to thermal stress in lizardite. Thermal effects causing expansion primarily along the *c* axis dominate over requirements to minimize O–H...O distances in the $2H_1$ polytype. In contrast, we tentatively conclude that optimum H-bonding is maintained *via* distortions of the ring of tetrahedra in the $1T$ polytype until about 300°C, after which thermal effects dominate. Presumably, where weaker interlayer bonding occurs, as in the $2H_1$ polytype, thermal effects dominate throughout the temperature range studied. A two-step process occurs in the $1T$ polytype because thermal motion becomes dominant at higher temperatures, where interlayer bonding weakens sufficiently, in part because of the inability of adjustments in the tetrahedral rings (*via* rotations) to maintain optimum H bonding across the interlayer.

Acknowledgements

Lizardite samples which were kindly provided by M. Mellini, Università di Siena, Italy. We appreciate discussions with R.T. Downs, University of Arizona, Tucson, Arizona, on rigid-body analysis. We thank M. Mellini and G. Cruciani for reviews.

References

Boscardin, M., Gentile, P. & Reposi, G. (1982): Ritrovamento di lizardite cristallizzata sul Monte dei Tre Abati nel Piacentino. *Natura* **73**, 173-182.

Brigatti, M.F., Galli, E., Medici, L. & Poppi, L. (1997): Crystal structure refinement of aluminian lizardite-$2H_2$. *Am. Mineral.* **82**, 931-935.

Brown, G.E., Sueno, S. & Prewitt, C.T. (1973): A new single-crystal heater for the precession camera and four-circle diffractometer. *Am. Mineral.* **70**, 698-704.

Cromer, D.T.& Mann, J.B. (1968): X-ray scattering factors computed from numerical Hartree–Fock wave functions. *Acta Crystallogr.* **A24**, 321-324.

Downs, R.T., Gibbs, G.V., Bartelmehs, K.L. & Boisen, M.B., Jr. (1992): Variations of bond lengths and volumes of silicate tetrahedra with temperature. *Am. Mineral.* **77**, 751-757.

_____, _____ & Boisen, M.B., Jr. (1990): A study of the mean-square displacement amplitudes of Si, Al, and O atoms in framework structures: evidence for rigid bonds, order, twinning, and stacking faults. *Am. Mineral.* **75**, 1253-1267.

Gillery, F.H. (1959): The X-ray study of synthetic Mg-Al serpentines and chlorites. *Am. Mineral.* **44**, 143-152.

Gregorkiewitz, M., Lebech, B., Mellini, M. & Viti, C. (1996): Hydrogen positions and thermal expansion in lizardite-1T from Elba: a low-temperature study using Rietveld refinement of neutron diffraction data. *Am. Mineral.* **81**, 1111-1116.

Guggenheim, S., Chang, Yu-Hwa & Koster van Groos, A.F. (1987): Muscovite dehydroxylation: high-temperature studies. *Am. Mineral.* **72**, 537-550.

Mellini, M. (1982): The crystal structure of lizardite 1T: hydrogen bonds and polytypism. *Am. Mineral.* **67**, 587-598.

_____ & Viti, C. (1994): Crystal structure of lizardite-1T from Elba, Italy. *Am. Mineral.* **79**, 1194-1198.

_____ & Zanazzi, P.F. (1987): Crystal structures of lizardite-$1T$ and lizardite-$2H_1$ from Coli, Italy. *Am. Mineral.* **72**, 943-948.

_____ & _____ (1989): Effects of pressure on the structure of lizardite-$1T$. *Eur. J. Mineral.* **1**, 13-19.

Nelson, D.O. & Guggenheim, S. (1993): Inferred limitations to the oxidation of Fe in chlorite: a high-temperature single-crystal X-ray study. *Am. Mineral.* **78**, 1197-1207.

Prewitt, C.T. & Finger, L.W. (1992): Crystal chemistry of high-pressure hydrous magnesium silicates. *In* High-Pressure Research: Applications to Earth and Planetary Sciences (Y. Syono & M.H. Manghnani, eds.). Terra Scientific Publishing, Tokyo and American Geophysical Union, Washington, D.C. (269-274).

Robinson, K., Gibbs, G.V. & Ribbe, P.H. (1971): Quadratic elongation: a quantitative measure of distortion in coordination polyhedra. *Science* **172**, 567-570.

Sales, K.D. (1987): Atomic scattering factors for mixed atom sites. *Acta Crystallogr.* **A43**, 42-44.

Siemens (1990): SHELXTL PLUS 4.0. Siemens Analytical X-Ray Instruments, Inc., Madison, Wisconsin.

Takeda, H. & Morosin, B. (1975): Comparison of observed and predicted structural parameters of mica at high temperature. *Acta Crystallogr.* **B31**, 2444-2452.

Received July 1, 1998, revised manuscript accepted December 7, 1998.